Spin–orbit splittings in Si/SiGe quantum wells: from ideal Si membranes to realistic heterostructures

2011 New J. Phys. 13 013009

(http://iopscience.iop.org/1367-2630/13/1/013009)

New Journal of Physics
The open-access journal for physics

Spin–orbit splittings in Si/SiGe quantum wells: from ideal Si membranes to realistic heterostructures

M Prada[1], **G Klimeck**[2] **and R Joynt**[1,3]

[1] Department of Physics, University of Wisconsin-Madison, WI 53706, USA
[2] Network for Computational Nanotechnology, Purdue University, W Lafayette, IN, USA
E-mail: rjjoynt@wisc.edu

New Journal of Physics **13** (2011) 013009 (18pp)
Received 19 June 2010
Published 11 January 2011
Online at http://www.njp.org/
doi:10.1088/1367-2630/13/1/013009

Abstract. We present a calculation of the wavevector-dependent subband level splitting from spin–orbit coupling in Si/SiGe quantum wells. We first use the effective-mass approach, where the splittings are parameterized by separating contributions from the Rashba and Dresselhaus terms. We then determine the inversion asymmetry parameters by fitting tight-binding numerical results obtained using the quantitative nanoelectronic modeling tool, NEMO-3D. We describe the relevant coefficients as a function of applied electric field and well width in our numerical simulations. Symmetry arguments can also predict the behavior, and an extensive analysis is also presented in this work. Using vast computational resources, we treat alloy disorder at the atomistic scale. We obtain first-time results for realistic Si/SiGe heterostructures. Our numerical data are in very good agreement with experimental results, both qualitatively and quantitatively. We conclude that effects of alloy disorder have a crucial influence on the spin–orbit parameters.

[3] Author to whom any correspondence should be addressed.

Contents

1. Introduction

Silicon is a leading candidate material for spin-based quantum information processing [1, 2]. Its spin–orbit coupling (SOC) is relatively weak and the hyperfine coupling can be eliminated by isotopic purification [3]. This means that the spin lifetimes should be long. One way to measure a spin lifetime is to use electron spin resonance (ESR) on two-dimensional electron gases (2DEGs) in silicon quantum wells (QWs) [4]–[6], where the D'yakonov–Perel (DP) mechanism accounts for the relaxation [7]. SOC may also be measured directly, using ESR [8, 9] or photocurrents [10]. To compare with experiment, however, we need the wavevector-dependent SOC Hamiltonian, which is best calculated atomistically. That is the aim of this paper. We shall focus on Si layers grown in the [001]-direction on $Si_{1-x}Ge_x$ substrate, with $Si_{1-x}Ge_x$ layers on either side, and on 'ideal' free-standing membranes.

Most calculations of the DP relaxation in Si [11, 12] have used the Rashba Hamiltonian [13], which is of the form

$$H_R = \alpha(E_z, N, v)(\sigma_x k_y - \sigma_y k_x). \tag{1}$$

σ_i are the Pauli matrices and k_i are the 2D wavevector components. N is the number of atomic Si layers in the well. v is the valley degree of freedom. We focus on the lowest electric subband, in which case the valley degree of freedom is two-valued [14] so that v is a two-by-two matrix.

$\alpha(E_z)$ depends (in lowest order) linearly on E_z, the external electric field, and often only this term is kept. E_z is of the order of $1\text{–}5 \times 10^7\ \mathrm{V\,m^{-1}}$ in heterostructures or MODFET devices [15]. The large magnitude of the field makes it important to examine the linearity assumption, and that is one of the purposes of this paper. H_R is generally thought of as a bulk term arising independently of the presence of the interfaces. However, de Andrade e Silva *et al* pointed out that surface effects may also be important [16], and this assumption will also be re-evaluated below.

In addition, a detailed treatment of the surface effects by Nestoklon *et al* in the absence of an applied field E_z showed that in this case one obtains a term

$$H_D = \beta(E_z, N, v)(\sigma_x k_x - \sigma_y k_y) \tag{2}$$

if N is odd [17, 18]. This is a Dresselhaus-like term [19] in that it arises from inversion asymmetry, although in contrast to the origin of this term in the asymmetry of the unit cell

in III–V materials, in Si layers it is due to the breaking of inversion symmetry *by the interfaces*. The lowest-order term in the power series expansion in E_z for $\beta(E_z, N, v)$ is a constant, so that if N is odd then we get a surface-induced spin splitting even in the absence of an external field. We will compute this term in an atomistic model of the solid.

The symmetry considerations refer to an ideal free-standing Si layer. Real heterostructures of $Si/Si_{1-x}Ge_x$ have substitutional disorder that destroys all symmetries: in these systems, α and β are always nonzero. Unlike all work done to date, our calculations will take the disorder of realistic structures into account. Previous works [17] present numerical calculations where the interfaces are introduced by using the virtual-crystal approximation. Since α and β have substantial contributions from atomic-scale interface effects, this is a rather crude approach. In contrast, our model includes atoms represented explicitly in the tight-binding model. Disorder is included by generating large unit cells that contain randomly distributed Ge atoms in the interfaces. Symmetry arguments and δ-functional theory allowed us to predict the qualitative behavior of the inversion asymmetry coefficients as a function of electric fields, E_z, well width, N, and valley degree of freedom, v.

The numerical tight-binding calculations are carried out with NEMO-3D [20] on nanoHUB.org computational resources[4]. In NEMO-3D, atoms are represented explicitly in the $sp^3d^5s^*$ tight-binding model, and the valence force field (VFF) method is employed to determine the atomic positions by minimizing the strain energy for each realization of the disorder [21]. NEMO-3D enables the calculation of localized states in a QW and their in-plane dispersion relation with a very high degree of precision, allowing us to extract the splittings along the in-plane directions in k space. The fourfold degeneracy of the states is split first by the valley splitting Δ_v and then by two smaller spin–orbit splittings, a splitting Δ_1 that is independent of the valley index v and a further splitting Δ_2 that depends on the valley index (see figure 2), allowing us to compute α and β.

In summary, the purpose of this paper is to determine the functions $\alpha(E_z, N, v)$ and $\beta(E_z, N, v)$ both for the ideal, free-standing case and for the case of a realistic well confined in an $Si/Si_{1-x}Ge_x$ heterostructure. These functions determine the spin properties of electrons in Si QWs. We shall focus particularly on the question of which term dominates for QWs with realistic values of E_z and N.

This paper is organized as follows. Section 2 discusses the symmetry operations of a silicon membrane and introduces expressions for the SOC in a δ-functional effective mass approach. Based on these symmetry and δ-functional arguments, we examine the effects of E_z, N and v on the inversion asymmetry coefficients, $\alpha(E_z, N, v)$ and $\beta(E_z, N, v)$, to give a qualitative and predictable picture. Section 3 contains the numerical results for ideal Si QWs: these are free-standing layers of silicon, for a varying number of atomic layers, N, and electric field, E_z. Results for realistic SiGe/Si/SiGe heterostructures are given in section 4. We conclude in section 5 with a summary of the results obtained.

2. Analysis of the spin–orbit coupling (SOC) in Si layers

2.1. Symmetry arguments

For clarity, we repeat and elaborate on the symmetry operations of this system in the ideal case [17], since they are far from obvious. The lattice considered as a bulk sample has a diamond

[4] Computational resource of a 256-node 3.3 GHz Pentium Irvindale PC cluster.

structure with a tetragonal distortion due to the $Si_{1-x}Ge_x$ layers: the [001]-axis along the growth direction is compressed relative to the in-plane [100] and [010] axes. The conventional unit cell has lattice constants a_x and a_z.

For a Si layer with an *odd* number N of atomic layers, we take the origin $(0, 0, 0)$ at an atom in the central plane. Mirror reflection in the $z = 0$ plane is not a symmetry, since it interchanges the $z = a_z/4$ and $z = -a_z/4$ layers, whose in-plane shift is $(a_x/2)(0, 1, 0)$. The $z = 0$ plane is also not a glide plane, since following the reflection by the translation of $(a_x/2)(0, 1, 0)$ to restore the $z = a_z/4$ and $z = -a_z/4$ layers would change the $z = \pm a_z/2$ layers. The 180° rotations about the z-axis passing through the origin is a symmetry of the layer, as are the reflections through the (110) and $(1\bar{1}0)$ planes. The eight operations take the point (x, y, z) into the points $\{(x, y, z), (x, -y, -z), (-x, y, -z), (-x, -y, z), (-y, x, -z), (y, -x, -z), (y, x, z)$ and $(-y, -x, z)\}$. Thus the point symmetries form the D_{2d} group and the space group is symmorphic. Spin–orbit effects come from terms linearly proportional to σ_i, the spin operators that transform as pseudovectors, while the electric field $\vec{E} = (0, 0, E_z)$ and in-plane momentum $\vec{k} = (k_x, k_y, 0)$ transform as vectors, the same as the coordinates. Our interest here is in combinations of these three quantities. Using the above list of operations, we find in zeroth order in E_z that there is one invariant term in the Hamiltonian, which has the Dresselhaus form $k_x\sigma_x - k_y\sigma_y$. In first order in E_z, there is only the Rashba term $E_z(k_x\sigma_y - k_y\sigma_x)$ (which is of course invariant under all isometries). Either of these terms can be multiplied by any even function of E_z, which is invariant under all the operations. Thus we find that when N is an odd number, $\beta(N, E_z, v)$ is an even function of E_z and $\alpha(E_z, N, v)$ is an odd function of E_z.

For a Si layer with an *even* number N of atomic layers, we take the origin $(0, 0, 0)$ at the center of a bond between atoms at positions $(a_x/8, a_x/8, a_z/8)$ and $(-a_x/8, -a_x/8, -a_z/8)$. The origin is a center of inversion. The rotation through 180° about the $(1\bar{1}0)$ axis is a symmetry operation. The (110) axis is a screw axis since the 180° rotation about this axis accompanied by a translation through $(a_x/4, a_x/4, 0)$ is a symmetry operation. The same is true for the 180° rotation about the (001) axis. The eight operations of the factor group take the point (x, y, z) into the points $\{(x, y, z), (-x, -y, -z), (-y, -x, -z), (y, x, z), (y + a_x/4, x + a_x/4, -z), (-y - a_x/4, -x - a_x/4, z), (-x + a_x/4, -y + a_x/4, z)$ and $(x - a_x/4, y - a_x/4, -z)\}$. Modulo translations are isomorphic to the group D_{2h}. Because of the appearance of the translations, this is not a true point group and the space group is not symmorphic. Its action in the Hilbert space reduces in many cases to projective rather than faithful representations of D_{2h}. However, this does not affect the symmetry analysis of the Hamiltonian. In zeroth order in E_z, the group does not allow any combination of terms of the form $k_i\sigma_j$, since all such terms change sign under inversion. In first order, the Rashba term $E_z(k_x\sigma_y - k_y\sigma_x)$ and a Dresselhaus term are both allowed. Again, multiplication of this expression by any even function of E_z is permissible. Thus, we find that when N is an even number, $\alpha(N, E_z, v)$ is an odd function of E_z and $\beta(E_z, N, v)$ is an odd function of E_z.

We stress once more that these symmetries will be violated in QWs confined between alloy layers. Even in the virtual crystal approximation, the alloys must be identical for any of the above operations that take z into $-z$ to be symmetries.

2.2. *δ-Functional theory of interface effects*

These considerations demonstrate that the interfaces have a profound effect on the SOC Hamiltonian. The interfaces have another important effect, which is to create valley splitting.

Recently, a multiscale theory of the valley effects has been constructed [22], which combines effective mass theory and tight-binding theory. In this subsection, we give an extension of this theory for the SOC Hamiltonian. The full SOC Hamiltonian contains both bulk and interface effects (unlike the valley Hamiltonian, which is zero in bulk). We shall not distinguish these effects, which are included on an equal footing in our calculations.

First recall that the sixfold degeneracy of the low-lying conduction electron states in Si is lifted by strain [14]. For a QW confined along z, the four valleys near $\vec{k} = (\pm k_0, 0, 0)$ and $\vec{k} = (0, \pm k_0, 0)$ rise in energy relative to the two z valleys near $\vec{k} = (0, 0, \pm k_0)$. The energy splitting from strain is large: values of a few hundreds of meV have been measured [23], so we expect only the lowest z valleys to play a role in typical low-temperature experiments. In the bulk, the two z-valleys are degenerate, but in QWs the interface potential mixes the two valleys and produces the valley splitting Δ_v.

In the envelope-function picture [24], the wavefunctions are written as

$$\Psi(\vec{r}) = \sum_{v=\pm s=\uparrow,\downarrow} \alpha_{v,s} \mathrm{e}^{\mathrm{i}nk_0 z} u_{\vec{k}}(\vec{r}) \Phi_{\vec{k},v,s}(z), \tag{3}$$

where $\alpha_{v,s}$ are the spin and valley mixing amplitudes, $u_{\vec{k}}(\vec{r})$ are the Bloch periodic functions and $\Phi_{\vec{k},v,s}(z)$ are the envelope functions. $\vec{k}$ is measured from the appropriate valley minimum. The valley index n takes the values + and −. We now model the interfaces at $z = z_d$ and $z = z_u$ as discontinuous potentials, i.e. as electric fields that are nonzero only in a vanishingly thin layer. The well thickness is given by $L = z_u - z_d$. The usual procedure for deriving the effective wave equation for Φ yields

$$\left[-\frac{\hbar^2}{2m_l} \frac{\mathrm{d}^2}{\mathrm{d}z^2} + V(z) + \Lambda(\vec{k})\delta(z - z_u) + \Lambda(\vec{k})\delta(z - z_d) \right] \Phi = E\Phi. \tag{4}$$

$V(z)$ is the part of the potential that is independent of valley and spin; it represents the external electric field E_z and the band gap offsets at the interfaces. (In Si/SiGe wells, the discontinuity in the mass is not important.) $\Lambda(\vec{k})$ is the residual interface potential; it is a matrix in the indices v and s. We treat only the case of identical interfaces; the extension to different interfaces is straightforward.

Introducing $s_0^{(vv')} = \delta_{vv'}$ $(i = 0)$ and $s_i^{(vv')}$ as the Pauli matrices $(i = 1, 2, 3)$ for the valley indices v, v' and $\sigma_0^{(tt')} = \delta_{tt'}$ $(j = 0)$ and $\sigma_j^{(tt')}$ $(j = x, y, z)$ as the Pauli matrices for the spin indices t, t', we see that in principle the Λs contain 16 real parameters $\lambda_{ij}(\vec{k})$, one for each combination of indices: $\Lambda = \sum_{i,j=0}^{3} \lambda_{ij}\, s_i \otimes \sigma_j$. We shall see that many fewer actually suffice, and in fact we can immediately note that $\lambda_{i3} = 0$ because of the transversality of SOC and $\lambda_{3j} = 0$ in the valley basis we have chosen. The unobservable constant λ_{00} can also be set equal to zero. We introduce the Λ, λ notation to indicate that all possible physical effects of the interfaces have been taken into account: the bispinor expansion of Λ is an expansion in a complete set for this 4-by-4 problem. We shall in practice relate the more commonly used coefficients α and β to atomistically calculated energy splittings.

The problem posed by equation (4) is solved by treating $-(\hbar^2/2m_l^2)(d^2/dz^2) + V(z)$ as the unperturbed Hamiltonian and the rest as a perturbation. This results in a spin- and valley-dependent kink in Φ at the interfaces. Alternatively, one may interpret the effect as a spin- and valley-dependent reflection at the interfaces, as was done by Nestoklon *et al* [17] (see figure 1(a)).

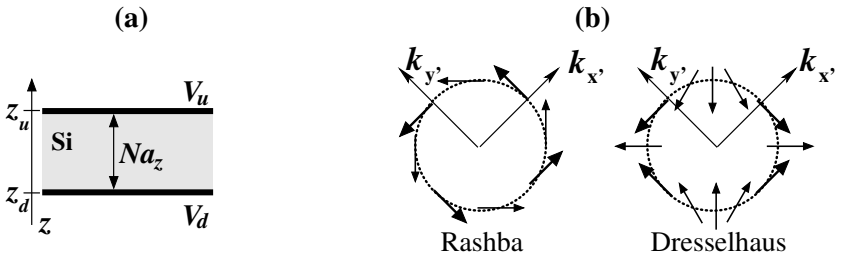

Figure 1. (a) Schematic representation of a Si QW: the potential is considered in the interfaces at z_u and z_d. (b) The Rashba and the Dresselhaus spin–orbit fields for different directions in $\boldsymbol{k}$ space: along the $\hat{x}'$ and $\hat{y}'$ directions, the eigenstates are parallel.

The spin-independent pure valley problem corresponds to the determination of the λ_{i0}. This has been worked out by Friesen *et al*, finding: $\lambda_{10} = v_v[\cos(2k_0 z_u)|\Phi_u|^2 + \cos(2k_0 z_d)|\Phi_d|^2]$ and $\lambda_{20} = v_v[\sin(2k_0 z_u)|\Phi_u|^2 + \sin(2k_0 z_d)|\Phi_d|^2]$. v_v is another microscopic parameter. This leads to a valley splitting $\Delta_v = \sqrt{\lambda_{10}^2 + \lambda_{20}^2}$. Since Δ_v is much greater than the SOC splittings, further simplification is possible, as we shall see below.

Following this approach, we can use the symmetry arguments to find a parameterization of the effective in-plane SOC Hamiltonian. We consider the high-symmetry directions $x' \parallel [110]$ and $y' \parallel [1\bar{1}0]$, along which the spin eigenstates are parallel (see figure 1(b)). This simplifies the analysis of the numerical calculations, as we shall see below. In this rotated basis, we have the interface-induced spin–orbit Hamiltonian: $H_{\mathrm{SO}}^{\mathrm{int}} = (\alpha_{\mathrm{int}} + \beta_{\mathrm{int}})\hat{\sigma}_{x'}k_{y'} + (\beta_{\mathrm{int}} - \alpha_{\mathrm{int}})\hat{\sigma}_{y'}k_{x'}$. Only the linear in k terms are taken into account, since the numerical results show that, for the electric fields considered in this work, the energy splittings appear to behave linearly with k.

We consider separately the parameters λ_{0j} $(j = 1, 2)$, which can be thought of as the 'intra-valley' SOC constants, and the parameters λ_{ij} $(i = 1, 2)$; $(j = 1, 2)$, the 'inter-valley' SOC: $H_{\mathrm{SO}} = H_{\mathrm{SO1}} + H_{\mathrm{SO2}}$, where H_{SO1} corresponds to $i = 0$ and H_{SO2} corresponds to $i = 1, 2$. The simplest way to think about the interfaces is that they introduce a local electric field: this transforms in the same way that E_z does, allowing us to use the above symmetry arguments to write down the expressions for the interface-induced Hamiltonians.

For the intra-valley contribution, H_{SO1}, we find

$$H_{\mathrm{SO1}} = s_0 k_{x'}\hat{\sigma}_{y'}[\beta_{\mathrm{int}}(E_z, N; 0) + \alpha_{\mathrm{int}}(E_z, N; 0)] + s_0 k_{y'}\hat{\sigma}_{x'}[\beta_{\mathrm{int}}(E_z, N; 0) - \alpha_{\mathrm{int}}(E_z, N; 0)]. \quad (5)$$

The main point now is that *the dependence on electric field E_z and layer number N can be found explicitly.* We treat the interfaces as local electric fields in the z-direction and use the transformation properties for E_z already given. In the case where the interfaces are identical (equal band offsets), this yields

$$\alpha(E_z, N; 0) \equiv \alpha_0 = a_0|(|\Phi_u|^2 - |\Phi_d|^2)|,$$
$$\beta(E_z, N; 0) \equiv \beta_0 = b_0|(|\Phi_u|^2 - (-1)^N|\Phi_d|^2)|.$$

Here, $\Phi_u \equiv \Phi(z_u)$ and $\Phi_d \equiv \Phi(z_d)$. a_0 and b_0 are real microscopic parameters that go beyond effective mass theory and that must be determined by an atomistic calculation. The dependence on the external field E_z is contained in $|\Phi_u|^2$ and $|\Phi_d|^2$. For nonzero E_z, these two quantities are different in magnitude. Note that the parity of N is contained in the Dresselhaus term,

which would be nonzero for N odd and $E_z = 0$ (or $|\Phi_u|^2 = |\Phi_d|^2$). This part of the in-plane Hamiltonian mixes spins in the same valley. We may determine the valley- and spin-part of the envelope function Φ by using the spin-independent part of the Hamiltonian as the unperturbed part. The eigenfunctions are in the literature [22]: in the basis $\{|\uparrow,+\rangle; |\downarrow,+\rangle; |\uparrow,-\rangle; |\downarrow,-\rangle\}$ they are $\varphi_{e,o} = (\mathrm{e}^{-\mathrm{i}\phi_v/2}, \mathrm{e}^{-\mathrm{i}\phi_v/2}, \pm\eta\mathrm{e}^{\mathrm{i}\phi_v/2}, \pm\eta\mathrm{e}^{\mathrm{i}\phi_v/2})$. The forms of η and ϕ_v are not so important here; they are given in [22]. Using the unperturbed solutions as the starting point for diagonalizing the intra-valley problem, we have $\Phi = F(z)\varphi$

$$\varphi^o_{\uparrow,\downarrow} \propto \begin{pmatrix} \mathrm{e}^{-\mathrm{i}(\phi_v+\phi_1)/2} \\ \pm\mathrm{e}^{-\mathrm{i}(\phi_v-\phi_1)/2} \\ -\mathrm{e}^{\mathrm{i}(\phi_v-\phi_1)/2} \\ \mp\mathrm{e}^{\mathrm{i}(\phi_v+\phi_1)/2} \end{pmatrix}, \quad \varphi^e_{\uparrow,\downarrow} \propto \begin{pmatrix} \mathrm{e}^{-\mathrm{i}(\phi_v+\phi_1)/2} \\ \pm\mathrm{e}^{-\mathrm{i}(\phi_v-\phi_1)/2} \\ \mathrm{e}^{\mathrm{i}(\phi_v-\phi_1)/2} \\ \pm\mathrm{e}^{\mathrm{i}(\phi_v+\phi_1)/2} \end{pmatrix}, \tag{6}$$

with $\phi_1(k_\pm) = \arg\{(1 \pm i))\mathrm{sgn}(\beta_0 \mp \alpha_0)\}$. Note that $\langle\varphi^i_\uparrow|\hat{\sigma}_{x'}|\varphi^i_\uparrow\rangle = -\langle\varphi^i_\downarrow|\hat{\sigma}_{x'}|\varphi^i_\downarrow\rangle = \pm 1$ or 0, depending on the phase ϕ_1, and likewise, $\langle\varphi^i_\uparrow|\hat{\sigma}_{y'}|\varphi^i_\uparrow\rangle = -\langle\varphi^i_\downarrow|\hat{\sigma}_{y'}|\varphi^i_\downarrow\rangle = 0$ or ± 1, so the eigenvectors are either eigenstates of $\hat{\sigma}_{x'}$ or $\hat{\sigma}_{y'}$, depending on the phase ϕ_1 given by the direction of the in-plane wave vector, $\vec{k}$. Along the $\hat{x}'$ or $\hat{y}'$ directions, the spin 'up' and 'down' states split in both valleys by the same amount, $|\varepsilon_\uparrow - \varepsilon_\downarrow| = \Delta_1 = 2|k|\,|(\beta_0 \pm \alpha_0)|$. Δ_1 is the part of the energy splitting that is independent of the valley index e, o.

We consider next the valley-mixing SOC, H_{SO2}, which contains the four coefficients λ_{ij} for $i = 1, 2$ and $j = 1, 2$. As previously noted by Nestoklon *et al*, a Si QW possesses mirror rotation operation $\mathcal{S}_4$, resulting in a relative phase change of $\phi_\alpha(\phi_\beta)$ for the Rashba (Dresselhaus) interaction at either interface. Combined with the absence (existence) of inversion center for even (odd) N, a change of sign is also observed in the Rashba (both the Rashba and the Dresselhaus) terms. Taking into account these symmetry arguments, the valley-mixing Hamiltonian has the form

$$H_{\mathrm{SO2}} = \sum_{i=x,y} s_i \left[\alpha(E_z, N; i)(\hat{\sigma}_{x'}k_{y'} - \hat{\sigma}_{y'}k_{x'}) + \beta(E_z, N; i)(\hat{\sigma}_{x'}k_{y'} + \hat{\sigma}_{y'}k_{x'})\right], \tag{7}$$

with

$$\begin{aligned}
\alpha(E_z, N; x) &= |a||(|\Phi_u|^2 - |\Phi_d|^2)\cos\phi_{0\alpha}, \\
\alpha(E_z, N; y) &= |a||(|\Phi_u|^2 + |\Phi_d|^2)\sin\phi_{0\alpha}, \\
\beta(E_z, N; x) &= |b||(|\Phi_u|^2 - (-1)^N|\Phi_d)|^2)\cos\phi_{0\beta}, \\
\beta(E_z, N; y) &= |b||(|\Phi_u|^2 + (-1)^N|\Phi_d|^2)\sin\phi_{0\beta},
\end{aligned}$$

where $\phi_0 = k_0 L$ and $\phi_{0i} = \phi_0 - \phi_i$. Again, a and b are microscopic parameters. We note that translation of the vector $\boldsymbol{r}$ by a three-dimensional Bravais-lattice vector $\boldsymbol{a}$ results in multiplication of the Bloch functions $|\pm\rangle$ by the factors $\exp(\pm\mathrm{i}k_0 L)$ [25], and thus a phase $\phi_0 = k_0 L$ appears in the valley-mixing terms,

$$H_{\mathrm{SO2}} = \frac{s_z}{2}[\hat{\sigma}_{y'}k_{x'}(\beta_z - \alpha_z) + \hat{\sigma}_{x'}k_{y'}(\beta_z + \alpha_z)], \tag{8}$$

with

$$\begin{aligned}
\alpha_z &= |a|(|\Phi_u|^2\cos\phi^-_\alpha - |\Phi_d|^2\cos\phi^+_\alpha) \\
\beta_z &= |b|(|\Phi_u|^2\cos\phi^-_\beta - (-1)^N|\Phi_d|^2\cos\phi^+_\beta),
\end{aligned}$$

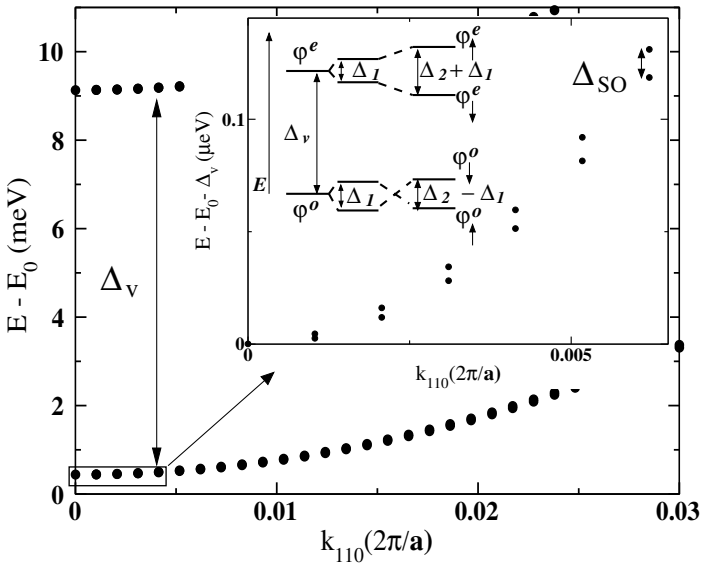

Figure 2. Splitting of levels due to spin mixing within the same valley and among different valleys. In the main diagram, the valley splitting is shown. The inset is on a much finer scale. The value of k in the inset is indicated by the vertical double-headed arrow: $k = 0.004\,(2\pi/a_x)$. Note that $\Delta_2 > \Delta_1$, in accordance with our numerical results.

where we have defined: $\phi_i^{\pm} = \phi_{0i} \pm \phi_v$. It is somewhat simpler to rotate the valley basis so that the e and o states are along the z'-axis. Hence, we can write the SOC Hamiltonian in a compact way, merging equations (5) and (8),

$$H_{\mathrm{SO}} = \hat{\sigma}_{y'} k_{x'} \sum_n \sum_{i=0,z'} \hat{s}_i [\beta_i^{(n)}(E_z, N) - \alpha_i^{(n)}(E_z, N)] + \hat{\sigma}_{x'} k_{y'} \sum_n \sum_{i=0,z'} \hat{s}_i [\beta_i^{(n)}(E_z, N) + \alpha_i^{(n)}(E_z, N)]. \tag{9}$$

Along $k_{x'}$ ($k_{y'}$), the eigenvectors are eigenstates of $\hat{\sigma}_{y'}$ ($\hat{\sigma}_{x'}$). The inter-valley term $i = z'$ has a relative change of sign for the splittings of the spin 'up' and 'down' states in either valley, $\Delta_2 = \pm 2k(\beta_z \pm \alpha_z)$, so there is a valley-dependent spin splitting, as depicted in the inset of figure 2: $|\varepsilon_\uparrow - \varepsilon_\downarrow| = |\Delta_2 \pm \Delta_1|$. From our numerical results, we observe that in general, $|\Delta_2| > |\Delta_1|$, causing a reversed symmetry in the spin structure in the lowest two valleys. We also observe that higher order terms contribute to the valley-mixing SOC, as well as intra-valley SOC in the heterostructure case. Hence, we have generalized equation (9) by labeling the order n of the interaction, so far considered to zero order: $\alpha^{(n)} \propto (k\alpha^{(0)})^2/|\varepsilon_n - \varepsilon_0|$. Note that the numerical results presented in this paper correspond to $\alpha = \sum_n \alpha^{(n)}$ and $\beta = \sum_n \beta^{(n)}$.

2.3. Qualitative picture for α and β

Beyond the symmetry arguments, we can also analyze the functions $\alpha(N, E_z, v)$ and $\beta(E_z, N, v)$ in qualitative terms. Let us first note that there are two distinct regimes for these functions considered in the E_z–N plane. In the weak-field (WF) or thick well regime, the wavefunction for the electrons in the lowest electric subband is spread throughout the well.

The strong-field (SF) or thin-well regime is reached when the wavefunction is confined near one interface and does not feel the other. In both the ideal and sandwich cases, the potential is rather flat in the interior of the well over a region whose extent $\sim N$ and the confinement comes from relatively sharp interfaces. In this case, placing the classical turning point in the middle of the well shows that the dividing line between the two regimes is described by

$$\text{(WF)} : E_z N^3 < \frac{32\hbar^2}{m_l e a_z^3} = 1.5 \times 10^{11} \frac{V}{m},$$

$$\text{(SF)} \ : E_z N^3 > \frac{32\hbar^2}{m_l e a_z^3} = 1.5 \times 10^{11} \frac{V}{m}.$$

m_l is the longitudinal mass. We need to consider the two sides of this line separately. Note that the SF case is more typical in real structures.

1. N dependence of $\alpha(E_z, N, v)$. For α the parity of N is not important. Let us define the lowest order term in E_z for $\alpha(E_z, N, v)$ as $\alpha^1(N, v)E_z(k_x\sigma_y - k_y\sigma_x)$. At first sight, the Rashba effect appears to be independent of the interfaces or the morphology of the structure, and therefore we expect $\alpha^1(N, v)$ to be independent of N. However, the Ehrenfest theorem implies that the expectation value of E_z, which is proportional to the mean force, must vanish for any wavefunction bound in the z-direction. Thus in a continuum effective mass approximation, the lowest-order term must vanish even though it is allowed by symmetry. Only when we put in interface effects and other atomic-scale effects will this term emerge. We shall assume that the extent of the interface in the z-direction is independent of N. If this is the case, then the probability of finding the electron at the interface in the WF regime is $\sim 1/N$, and we may expect $\alpha(E_z, N, v)$ to be a decreasing function of N in the WF regime. In the SF regime (large N) α becomes independent of N for fixed E_z since we only add layers that are unoccupied.

2. E_z dependence of $\alpha(E_z, N, v)$. We have seen that at small E_z (WF) the dependence on E_z is linear. At large E_z for fixed N (SF) the wavefunction is increasingly squeezed onto the interface and we may expect some continued increase in α. Hence, we can set

$$\alpha(E_z, N, v) = \alpha_1(N, v) \cdot E_z.$$

3. N dependence of $\beta(E_z, N, v)$.

(a) N odd. This is the only case for which $\beta(E_z = 0, N, v) \neq 0$. In the WF regime, this field-independent term may be considered as a perturbation in $1/N$, since it is zero for even N and the adding of an additional layer to make N odd is the same as adding a term to the Hamiltonian whose matrix elements vanish as $1/N$. So, we expect an initial decrease in the term as a function of N. Again, α should approach a constant at large $N$and fixed E_z for the same reasons as in 1.

(b) N even. $\beta(E_z = 0, N, v) = 0$. In the WF regime, the field-independent term should converge to the result for even N as N increases, since they differ by terms of the order of $1/N$. The same holds for the SF regime.

4. E_z dependence of $\beta(E_z, N, v)$.

(a) N odd. There is a constant term but no strong dependence on E_z in the WF regime. In the SF regime, the wavefunction is strongly confined to the interface. If we consider just a two-layer interface, there is a very strong orthorhombic anisotropy: the [110] and [1$\bar{1}$0] directions are different, since the nearest-neighbor bond is in one of the two directions. Hence $\beta(E_z, N, v)$ can be expected to be large, so $\beta(E_z, N, v)$ should increase strongly at large E_z with fixed N.

(b) N even. In the WF regime, the symmetry is very important and $\beta(E_z, N, v)$ is linear in E_z. Again, in the SF regime we expect to converge to the odd N result.

Finally, we consider the v dependence. The valley splitting Δ_v vanishes in the effective-mass continuum approximation—it is due to interface effects. For $E_z = 0$, the eigenfunctions must be even in z: $\psi_+(r) = F(z)\phi(\vec{r})\cos k_0 z$ or odd in z: $\psi_-(\vec{r}) = F(z)\phi(\vec{r})\sin k_0 z$, where $F(z)$ is an even, slowly varying envelope function and $\phi(\vec{r})$ is an even (in z) Bloch function. k_0 is the wavevector of the conduction-band minima. For a well with smooth surfaces such as we consider here, E_v has the order of magnitude ∼1–10 meV and oscillates with thickness on the scale $\Delta N = \pi/2k_0 a_z$ and is proportional to $1/N$, as expected for an interface effect in the WF regime. In the SF regime, $E_z \neq 0$ and the eigenstates are no longer even or odd. Δ_v saturates for large N at fixed E_z, and its overall magnitude increases with E_z, also as expected as the wavefunction is squeezed onto an interface.

The oscillations with N arise in the following way. Let $V(z)$ be the confining potential and $V(k)$ its Fourier transform: $V(k) = \int \exp(\mathrm{i}kz)V(z)\,\mathrm{d}z$. If we apply lowest-order degenerate perturbation theory for states in the two valleys, we find $\Delta_v = \left|\int \mathrm{d}^3 r\ F^2(z)\phi^2(\vec{r})\mathrm{e}^{2\mathrm{i}k_0 z}V(z)\right| \sim |V(2k_0)|$. As we change N, $V(z)$ has variation on the scale $z = 4Na$, the separation between the two interfaces. $|V(2k_0)|$ then has constructive interference when $2k_0 \times 4(\Delta N)a = 2\pi$ or $\Delta N = \pi/4k_0 a$. This ignores Umklapp, which will be present in the actual system, but is absent in the tight-binding approximation. It turns out that the dependence on the valley index can be quite dramatic. The valley states differ substantially right at the interface, where much of the spin–orbit effect arises. By the same token, we can expect the same oscillations with N that are seen in Δ_v to be present in Δ_{SO}, the spin–orbit energy splitting.

In actual heterostructures, the interfaces are not sharp. Ge is substituted for Si on randomly chosen sites, which will generally mean that the penetration length of the wavefunctions into the barriers varies randomly in x and y. All symmetries are violated by the disorder and it no longer makes clear sense to speak of even and odd N. Furthermore, the free electrons come from dopants that create an electric field in the structure, so that the $E_z = 0$ limit is not accessible. It will probably be very difficult to observe the parity dependences that are predicted from symmetry arguments and also the oscillations. However, it may be possible to observe such effects in free-standing membranes.

3. Results for the ideal case

In this section, we get the tight-binding results for the free-standing layer. We impose hard wall boundary conditions at both interfaces and perform tight-binding calculations to obtain the eigenvalues and eigenvectors. Our approach to determining α and β will be to compute Δ_{SO} along [110] and [1$\bar{1}$0] using NEMO-3D for free-standing layers with varying thickness N and applied electric field E_z. To discriminate the Rashba and the Dresselhaus contributions, we also compute the expectation value of $\sigma_{x'}$ and $\sigma_{y'}$, which determines ϕ_1 of equation (6) and thus the sign of $(\beta - \alpha)$.

The case $N = 60$ is shown in figure 2. We show the four energy eigenvalues of the lowest electric subband as a function of wavevector in the [110] direction for an 8 nm layer; this corresponds to $N = 60$, and $E_z > 0$. The valley splitting is about 9 meV, which is much larger than the spin–orbit splitting for all k. It is seen that Δ_{SO} is linear in k at small k. Extracting Δ_2 and Δ_1 (see diagram in the inset of figure 2), we can then calculate $(\beta + \alpha)$ and $(\beta - \alpha)$ from the slopes of these lines, which allows us to determine $\alpha_i(E_z = 0, N)$ and $\beta_i(E_z = 0, N)$ (see equation (9)).

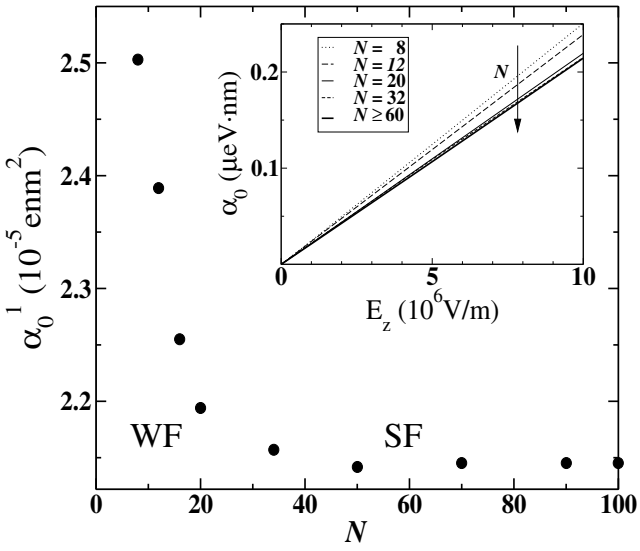

Figure 3. The intra-valley Rashba SOC coefficient α_0^1 for a free-standing Si layer as a function of thickness N (N is the number of atomic layers). Inset: α_0 as a function of E_z for different QW thicknesses.

The dependence of the intra-valley Rashba coefficient α_1^0 on E_z and N is shown in figure 3. We use the same procedure as for fixed N: the splittings are computed as a function of k in two different directions and the slopes yield α and β. The symmetry arguments imply that the α_0^1 should be linear in E_z, $\alpha_0(E_z, N) \approx \alpha_0^1 E_z$, and insensitive to N in the SF regime. The inset of figure 3 shows that this is the case. As a function of N, we see that α_1^0 is a decreasing function of N and then becomes insensitive to N in the SF regime.

For the Dresselhaus contribution, we separate the N even and odd cases. For N even, we do not observe any SOC-related terms at $E_z = 0$, as expected: we recall that any term of the form $k_j \sigma_i$ is forbidden by D_{2h} symmetry. We expect the terms to be linear to lowest order of E_z, which is indeed the case: $\beta_{0(z)} \simeq \beta_{0(z)}^1 E_z$. The results for the intra-valley coefficient β_0^1 are shown in figure 4. The SF value for the intra-valley coupling constant is $\beta_0^1 \simeq 8 \times 10^{-5}\,\mathrm{nm}^2$. We note an abrupt change in β_0^1 accompanied by a parity flip (depicted in the inset of figure 4), an event that has already been noted in the literature [26]–[29]. This reveals that β_0^1 is more sensitive to higher energy contributions than α_0.

The inter-valley parameters are plotted next. We observe again a linear behavior with electric field for both terms, as expected from the symmetry arguments. Figure 5 shows the linear coefficients, (a) α_z^1 and (b) β_z^1 (note that $\alpha_z = \alpha_z^1 E_z$ and $\beta_z = \beta_z^1 E_z$). Recall that under the D_{2h} operations, both the Rashba (for any N) and the Dresselhaus SOC (for even N) transform in a similar manner; hence a similar behavior is expected with E_z. We observe that both contributions exhibit oscillations as a function of N. These oscillations are related to the valley-splitting oscillations, already observed in the literature [17, 22, 25, 29, 30]. For large N, the interaction converges to the SF limit value: $\alpha_z^1 \sim 1.3 \times 10^{-5}\,\mathrm{nm}^2$ and $\beta_z^1 \sim 155 \times 10^{-5}\,\mathrm{nm}^2$.

These results lead to two significant conclusions: (i) the Rashba inter- and intra-valley contributions are of the same order of magnitude, which would indicate that the interface-independent part of α compares to the interface-induced part in the SF regime. In contrast, β_z^1 is more than one order of magnitude larger than β_z^0, indicating that it is a pure interface effect,

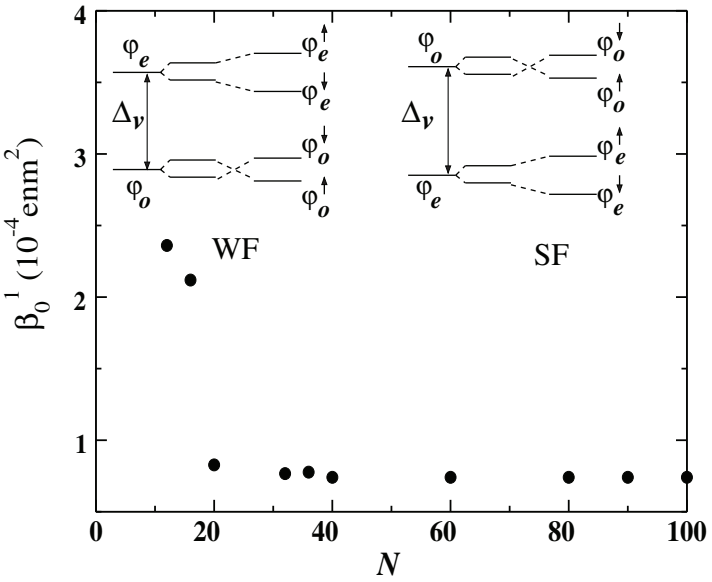

Figure 4. The intra-valley Dresselhaus coefficient β_0^1 as a function of N, for N even, in a free-standing Si layer. The insets show the valley–spin symmetry of the four lowest conduction subbands: a parity flip occurs at $N \sim 20$.

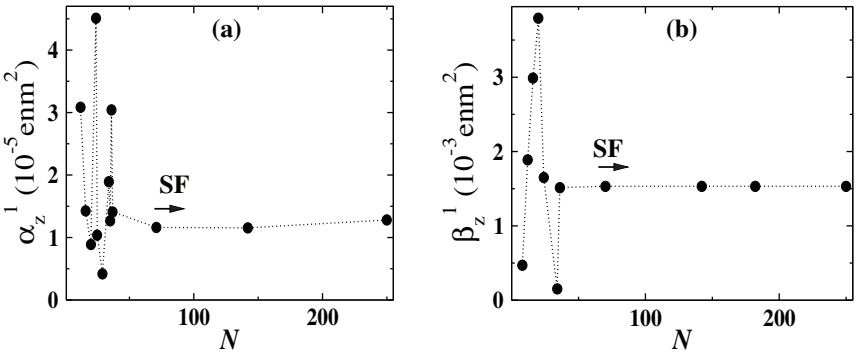

Figure 5. Intervalley SOC coefficients for free-standing Si layers as a function of well width N. (a) The Rashba coefficient α_z^1 and (b) the Dresselhaus coefficient β_z^1. The arrows indicate the beginning of the SF regime.

also sensitive to higher order energy levels. (ii) We also find from figures 3–5 that the dividing line between the SF and WF regimes is at $N \sim 50$, for which the linear coefficients β_i^1 and α_i^1, $i = 0, z$, are almost fixed as N increases. We choose $E_z \sim 10^6$–10^7 V m^{-1}, since this is the electric field range we use for our numerical calculations. This gives $E_z N^3 \sim 10^{11}$–10^{12} V m^{-1}, which is in very good agreement with our qualitative picture given in section 2.3.

Next, we consider the Dresselhaus contribution for N odd. Figure 6 shows β_0 as a function of E_z for different N. We observe that for large N, the parity effect is less apparent, and β_0 becomes independent of N, as predicted from our qualitative arguments. In the WF regime, β_z is not as sensitive as β_0 to electric fields. We note that $\beta_0(E_z = 0)$ is nonzero, as shown in the inset of figure 6. It presents strong oscillations with N in the WF regime, due to mixing with

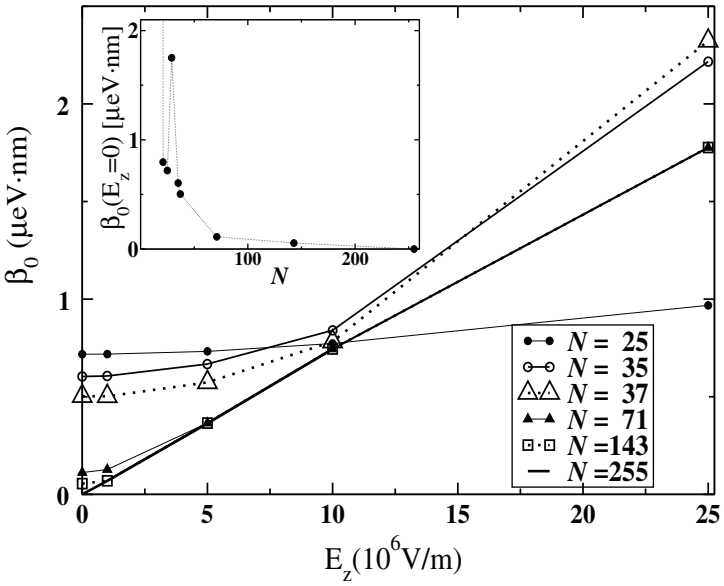

Figure 6. The intervalley Dresselhaus coefficient β_0 for a free-standing Si layer as a function of electric field E_z and well width N. The inset shows the zero-field value as a function of N.

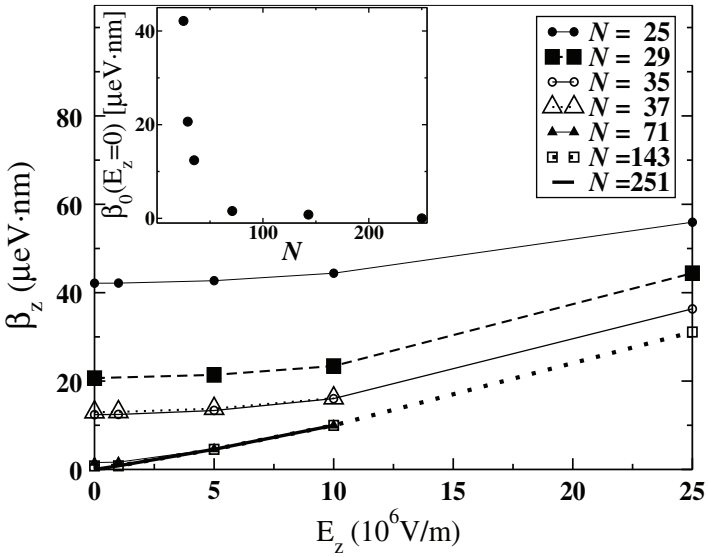

Figure 7. Intervalley Dresselhaus SOC contributions to splittings of the first subbands in Si QWs as a function of E_z, for N odd. The inset shows the zero-field value $\beta_z(E_z = 0)$ as a function of N.

higher energy states, and vanishes in the SF regime, as expected in the bulk limit for silicon. The overall $\beta_0^0(E_z = 0) \sim 1/N$ dependence is also evident in this curve.

The inter-valley Dresselhaus coupling constant for N odd is shown in figure 7. For large N, β_z becomes linear with E_z, as it corresponds to the bulk limit. The behavior is quite similar to β_0.

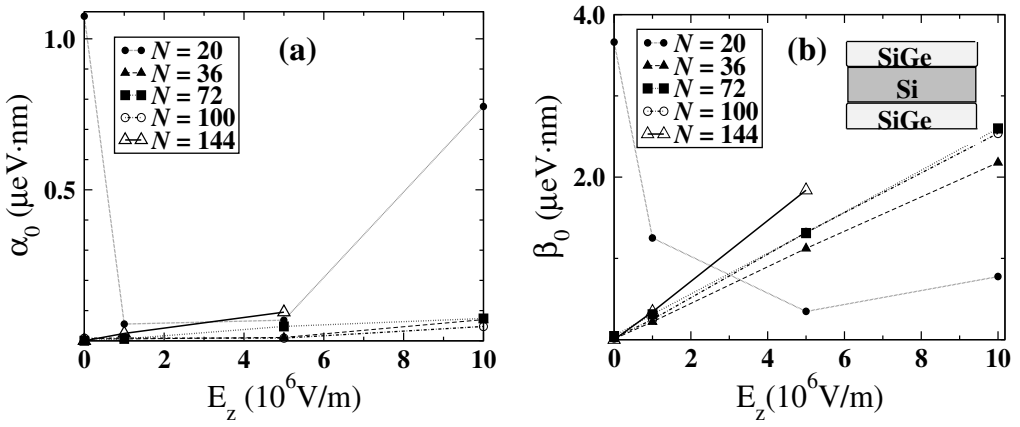

Figure 8. Intravalley SOC coefficients for a $Si_{1-x}Ge_x/Si/Si_{1-x}Ge_x$ ($x = 0.5$) QW as a function of E_z: (a) the Rashba coefficient α_0 and (b) the Dresselhaus coefficient β_0 for different numbers of atomic layers of Si, N. The inset of (b) is a sketch of the SiGe/Si/SiGe structure. •, $N = 20$; ■, $N = 36$; ▲, $N = 72$; ◦, $N = 108$; △, $N = 144$.

4. Results for heterostructures

Having verified that the results make physical sense overall, we redo the calculations for two more realistic models of an actual heterostructure. Firstly, we present the results on an $Si_{1-x}Ge_x/Si/Si_{1-x}Ge_x$ QW with $x = 0.5$. The Si layer is surrounded by 28 layers of $Si_{1-x}Ge_x$ on both sides. Our numerical results indicate that it is sufficient to avoid artificial surface effects and to confine the wavefunction in the Si QW for the electric fields presented here. Secondly, we investigate the most experimentally relevant case: a $Si_{1-x}Ge_x/Si/Si_{1-x}Ge_x$ structure grown on a $Si_{1-x}Ge_x$ substrate, with $x = 0.3$. Biaxial (shear) strain energy is minimized using VFF, which includes precise values of the elastic constants c_i. The unit cell is chosen to have 24 atomic layers along the [010] and [100] directions. Wider unit cells give similar results, indicating that on this limit realizations of the substitutional disorder are averaged over, ensuring the reliability of our results. These calculations are much more time-consuming than those for the free-standing layer, so fewer results are presented here. We stress that calculations of this kind have not been done previously. Earlier work used the virtual-crystal approximation for the outer layers, which artificially preserves the symmetry. The reduction in symmetry can only increase the number of possible terms in the Hamiltonian, so not only the Rashba and the Dresselhaus terms exist, but in principle all terms $k_i\sigma_j$ can exist—strictly speaking even k_x and k_y are no longer good quantum numbers. However, we shall take advantage of the approximate symmetry to present the results in the same way.

Figure 8 shows the parameters α_0 (a) and β_0 (b) as a function of electric field, E_z. We stress that the dramatic dependence on the parity of N is no longer present, i.e. we do not need to separate the even and odd N cases as in the previous section, since the disorder destroys their distinct symmetry properties. We also note that α is always nonzero, even for $E_z = 0$. The intravalley α_0 is nonlinear in the WF regime, reaching a linear-in-E_z value comparable to the one of Si QW in the SF regime (open triangles), $\alpha_0^1 \sim 1.9 \times 10^{-5}$ nm^2. This is consistent with the value obtained above for the Si QW.

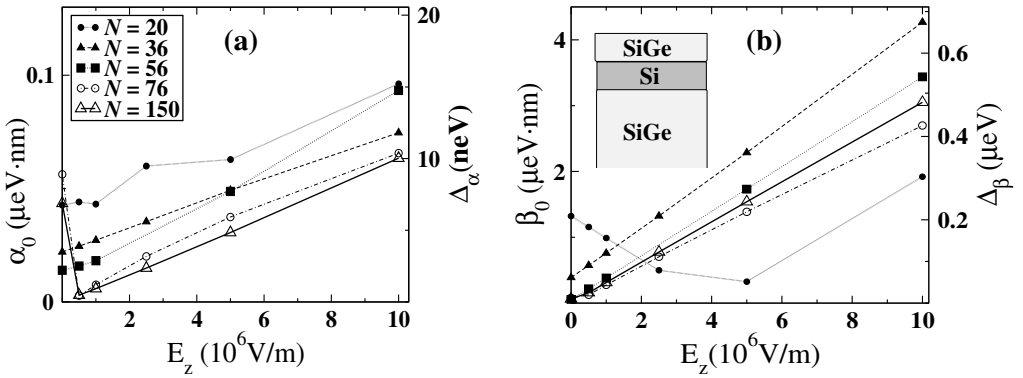

Figure 9. Intra-valley SOC coefficients for an $Si_{1-x}Ge_x/Si/Si_{1-x}Ge_x$ structure formed on a $Si_{1-x}Ge_x$ substrate, with $x = 0.3$. The Rashba (a) and Dresselhaus (b) contributions are shown as a function of E_z for different number of atomic layers of Si, N. The right vertical axis shows the absolute energy values of the splitting, calculated for the Fermi level of a typical Si QW with $n_s = 4 \times 10^{11}\,\mathrm{cm}^{-2}$ [31]. The inset of (b) sketches the structure: a Si layer is grown on a SiGe substrate and capped with a SiGe layer.

Figure 8(b) shows an overall $1/N$ dependence of β_i for $E_z = 0$, consistent with the previous section results and with the qualitative picture of section 2.3.3. For large N we observe that β_0 is linear with electric fields. We fit QW in the 10–30 nm range and find $\beta_0^1 \simeq 38 \times 10^{-5}\,\mathrm{nm}^2$. We also find, for the SF regime, $\beta_z^1 \simeq 58 \times 10^{-5}\,\mathrm{nm}^2$, with $\beta_i = \beta_i^1 E_z$.

We have also studied the eigenvectors for each case and find frequent parity-flips (see the inset of figure 4) by varying N or E_z. As a consequence, both β and α depend on N even in the SF regime.

Finally, we show the results for the $Si_{1-x}Ge_x/Si/Si_{1-x}Ge_x$ structure grown on a $Si_{1-x}Ge_x$ substrate, with $x = 0.3$. The in-plane lattice constant $a_\parallel$ is now relaxed to the SiGe. We apply fixed boundary conditions for the lattice constant to the SiGe value at the bottom of the QW, and allow NEMO-3D to minimize the strain energy by varying the lattice constant along the z-axis.

Figure 9 shows the linear-in-$\boldsymbol{k}$ SOC intra-valley contributions. The splittings are linear in E_z in the SF limit, although parity flips and higher energy levels result in small nonlinearities. We note, however, that the zero field shows a visible splitting, even for wide QWs ($N \sim 140$). We observe that α_0 is much smaller than in the previous samples, where silicon was the dominant component. For a typical Si/SiGe heterostructure with $n_s = 4 \times 10^{11}\,\mathrm{cm}^{-2}$ [31] we have $k_F \simeq 0.16\,\mathrm{nm}^{-1}$, at which the Dresselhaus-induced SOC splitting is $\Delta_\beta \simeq 1.25\,\mu\mathrm{eV}$, whereas the Rashba splitting is only $0.02\,\mu\mathrm{eV}$. Observing figure 9, we see the dividing line between the WF and SF regimes again at $N \gtrsim 50$ and $E_z \sim 10^6\,\mathrm{V\,m}^{-1}$, in agreement with our expectations (see section 2.3).

We show in table 1 the linear SOC coefficients for a 20 nm Si QW ($N \sim 140$) in the three different structures considered in this paper. α_i^1 and β_i^1 are in units of $10^{-5}\,\mathrm{nm}^2$. Note that the Dresselhaus term is dominant in all cases. The Rashba inter- and intra-valley coefficients are of similar order of magnitude for the membranes, although the latter is a factor of two larger in heterostructures. For the Dresselhaus coefficients, the inter-valley parameter is in general larger, being the dominant source of spin–orbit splitting.

Table 1. α_i^1 and β_i^1 $(i = 0, z)$ numerical results for 20 nm Si QW in the three different fashions considered in this paper, all in units of $10^{-5}\,\mathrm{nm}^{-2}$.

$\alpha_i^1(\beta_i^1)$ $(\times 10^{-5}\,\mathrm{nm}^{-2})$	α_0^1	α_z^1	β_0^1	β_z^1
'Pure' Si membrane	2.1	1.3	8.0	154.5
SiGe/Si/SiGe membrane	1.9	2.5	37.7	58.5
Si QW on SiGe substrate	0.7	1.5	30.6	97.8

Finally, we compare the results obtained above with experimental results [1]. Their experimental results give a linear-in-E_z term of $\simeq 5.5 \times 10^{-12}\,\mathrm{eV\,cm}$. We identify this with our β, the dominant linear in field spin–orbit parameter. Our tight-binding calculation for a 20 nm thick heterostructure yields the same value for a field of $\simeq 0.5 \times 10^7\,\mathrm{V\,m}^{-1}$. This field is in good agreement with the band structure of figure 1 of Wilamowski *et al* [1]. We stress that Nestoklon *et al* underestimated their spin–orbit coefficient (or overestimated their electric field, to $\simeq 0.3 \times 10^{10}\,\mathrm{V\,m}^{-1}$). Although built-in electric fields are difficult to measure, our value agrees with the ones assumed elsewhere [32, 33], which give 0.9 and $0.5 \times 10^7\,\mathrm{V\,m}^{-1}$, respectively. We conclude that the effects of disorder have indeed a crucial influence in the results.

5. Conclusions

We have been able to extract the **k**-dependent energy splittings in Si heterostructures due to SOC using an $\mathrm{sp^3d^5s^*}$ tight-binding model capable of taking into account the interface effects at the atomic scale. Our numerical data agree very well with experimental results [1], both quantitatively and qualitatively: the dominant contribution to spin–orbit splitting is the Dresselhaus one, which is linear in E_z and yields a value in agreement with Wilamowski *et al*, in contrast to previous calculations.

We also studied in detail the ideal case: for an Si QW, we distinguish the N even and odd cases, since the symmetry operation properties of the Dresselhaus-type terms are fundamentally different: While for N odd the Dresselhaus term appears at zero order in E_z, for N even it is linear in E_z to lowest order (as Rashba-type terms are). We have extracted the linear-in-E_z and **k**-linear parameters for the N even case.

We also distinguish two regimes of operation for typical wells: in the WF regime, the splittings vary strongly as a function of N. The intra-valley splittings show roughly a $1/N$ behavior, whereas the valley-mixing ones present also oscillations. In contrast, the splittings do not change with N in the SF limit. In general, the strength of the Dresselhaus term is more highly dependent on N than the Rashba term. Together with the oscillations observed for the intra-valley mixing, this suggests that higher-energy states are also very important. We also observe a reversed spin structure in the spin-split valleys, a direct consequence of the inter-valley splitting being larger than the intra-valley.

We have also studied the lowest energy eigenstates and found frequent parity flips when varying N or E_z. This might manifest itself in experiment by a strong sample-dependent SOC. In agreement with [17], we find that the energy splittings due to Dresselhaus are in general larger than Rashba-type ones: the Dresselhaus parameter β is almost one order of magnitude

larger than the Rashba α for the ideal (pure Si QW) case and roughly two orders of magnitude larger for the heterostructure (Si on SiGe substrate) case. We also find that the inter-valley contribution to spin–orbit splitting is generally larger than the intra-valley one. We recall, however, that throughout this paper the numerical data have been obtained for QWs with flat interfaces along a main crystallographic axis. More realistic samples include a small tilted angle with respect to a high symmetry axis. We have not performed calculations for this case; however, we expect the interface-induced Dresselhaus parameter β to become smaller in tilted samples in a similar manner as valley splitting does [33]. Since Rashba has a bulk component, it would not be affected as much by the tilt and we expect that α would remain of the same order of magnitude even in realistic tilted samples. Simulations carried out on a thin membrane confirm this hypothesis, although a more extensive study would quantitatively determine the SOC parameters.

Finally, we found that SOC is indeed weak in Si as compared to other materials: it is a few orders of magnitude smaller than in similar InGaAs or InAs-based structures [34]–[36], making Si a leading candidate for quantum information processing. We note that SOC would ultimately determine the spin lifetimes on an isotopically purified sample [3]. For emerging technologies like Si spintronics and quantum computing, it is therefore crucial to develop a predictive theory to determine SOC parameters.

Acknowledgments

We thank N Kharche, M Friesen and M Eriksson for useful conversations. This work was supported by the Spanish Ministry of Education and Science (MEC). Financial support was provided by the National Science Foundation, grant numbers NSF-ECS-0524253 and NSF-FRG-0805045, and by ARO and LPS, grant no. W911NF-08-1-0482.

References

[1] Wilamowski Z, Jantsch W, Malissa H and Rössler U 2002 *Phys. Rev.* B **66** 195315
[2] Tahan C, Friesen M and Joynt R 2005 *Phys. Rev.* B **66** 035314
[3] Prada M, Blick R and Joynt R 2010 *Physica* E **42** 639
[4] Wilamowski Z and Jantsch W 2004 *Phys. Rev.* B **69** 035328
[5] Tyryshkin A M, Lyon S A, Schenkel T, Bokor J, Chu J, Jantsch W, Schäffler F, Truitt J L, Coppersmith S N and Eriksson M A 2006 *Physica* E **35** 256
[6] Truitt J L *et al* 2008 Electron spin resonance and related phenomena in low dimensional structures *Topics in Applied Physics Series* vol 115 ed M Fanciulli (New York: Springer)
[7] D'Yakonov M I and Perel V I 1971 *Sov. Phys. JETP* **13** 1053
[8] Wilamowski Z, Malissa H, Schäffler F and Jantsch W 2007 *Phys. Rev. Lett.* **98** 187203
[9] Meier L, Salis G, Shorubalko I, Gini E, Schön S and Ensslin K 2007 *Nat. Phys.* **3** 650
[10] Ganichev S D *et al* 2004 *Phys. Rev. Lett.* **92** 256601
[11] Sherman E Y 2003 *Phys. Rev.* B **67** 161303(R)
[12] Ganichev S D *et al* 2002 *Phys. Rev.* B **66** 075328
[13] Bychkov Y A and Rashba E I 1984 *J. Phys. C: Solid State Phys.* **17** 6039
[14] Herring C and Vogt E 1956 *Phys. Rev.* **101** 9440
[15] Tahan C and Joynt R 2005 *Phys. Rev.* B **71** 075315
[16] de Andrada e Silva E A, La Rocca G C and Bassani F 1997 *Phys. Rev.* B **55** 16293
[17] Nestoklon M O, Ivchenko E L, Jancu J M and Voisin P 2008 *Phys. Rev.* B **77** 155328

[18] Winkler R 2003 *Spin-Orbit Coupling Effects in Two-Dimensional Electron and Hole System* (New York: Springer)
[19] Dresselhaus G 1955 *Phys. Rev.* **100** 580
[20] Klimeck G, Oyafuso F, Boykin T B, Bowen R C and von Allmen P 2002 *Comput. Model. Eng. Sci.* **3** 601
[21] Keating P N 1966 *Phys. Rev.* **145** 637
[22] Friesen M, Chutia S, Tahan C and Coppersmith S N 2007 *Phys. Rev.* B **75** 115318
[23] Schäffler F 1997 *Semicond. Sci. Technol.* **12** 1515
[24] Kohn W 1957 *Solid State Physics* vol 5 (New York: Academic) p 257
[25] Nestoklon M O, Golub L E and Ivchenko E L 2006 *Phys. Rev.* B **73** 235334
[26] Chiang J-C 1994 *Japan J. Appl. Phys.* **33** L294
[27] Boykin T B, Klimeck G, Eriksson M, Friesen M, Coppersmith S N, von Allmen P, Oyafuso F and Lee S 2003 *Appl. Phys. Lett.* **84** 115
[28] Boykin T B, Kharche N and Klimeck G 2008 *Phys. Rev.* B **77** 245320
[29] Boykin T B, Klimeck G, Friesen M, Coppersmith S N, von Allmen P, Oyafuso F and Lee S 2004 *Phys. Rev.* B **70** 165325
[30] Jancu J M, Scholz R, de Andrada e Silva E A and La Rocca G C 2005 *Phys. Rev.* B **72** 193201
[31] Shaji N *et al* 2007 *Nat. Phys.* **4** 540
[32] Goswami S *et al* 2007 *Nat. Phys.* **3** 41
[33] Kharche N, Prada M, Boykin T B and Klimeck G 2007 *Appl. Phys. Lett.* **90** 092109
[34] Nitta J, Akazaki T, Takayanagi H and Enoki T 1997 *Phys. Rev. Lett.* **78** 1335
[35] Heida J P, van Wees B J, Kuipers J J, Klapwijk T M and Borghs G 1998 *Phys. Rev.* B **57** 11911
[36] Hu C M *et al* 1999 *Phys. Rev.* B **60** 7736